Journal of MATERIALS RESEARCH

Review
DOI:10.1557/s43578-022-00539-9

EARLY CAREER SCHOLARS IN MATERIALS SCIENCE 2023

ANNUAL ISSUE

A review on chemical bath deposition of metal chalcogenide thin films for heterojunction solar cells

Sucheta Sengupta[1,a], Rinki Aggarwal[1], Manoj Raula[2]

[1] Amity Institute of Advanced Research and Studies (Materials and Devices), Amity University, Sector-125, Noida 201301, India
[2] Department of Chemistry, Amity Institute of Applied Sciences, Amity University, Sector-125, Noida 201301, India
[a] Address all correspondence to this author. e-mail: ssengupta1@amity.edu

Received: 30 November 2021; accepted: 10 March 2022; published online: 25 March 2022

Heterojunction (HJ) thin-film II–VI solar cells are emergent substitutes to the traditional silicon solar cells because of improved efficiency and cost-effectiveness. A renewed interest in depositing the constituent layers employing chemical bath deposition (CBD) is shown because of the absence of any stringent reaction conditions which ensures the preservation of the properties of the constituent layers. Variation in the growth conditions has strong effects on the morphologies and the properties of the resultant films specially the interface. Inappropriate or alloyed interfaces may result in pinholes formation affecting the resultant electric field because of reduced junction area and enhanced recombination for carriers which in turn affects the efficiency. In this review, we provide an overview of the different combinations of metal chalcogenide/chalcopyrite thin-film layers for HJ solar cells by CBD and achieving control over the resultant morphology, particularly focusing on interfacial epitaxial relationship which is found to have substantial influence on the efficiency of the resultant cell.

Sucheta Sengupta

Sucheta Sengupta Dr. Sucheta Sengupta is Assistant Professor and DST Inspire Faculty Fellow in the Department of Amity Institute of Advanced Materials and Research (Materials and Devices). She received her Bachelor's Degree in Chemistry from Presidency College under University of Calcutta, and a Master's degree from the Indian Association for Cultivation of Science and S. N. Bose National Centre for Basic Sciences, Kolkata, India, in 2007. She completed PhD at the Centre for Advanced Materials, Indian Association for Cultivation of Science in 2013, under the supervision of Professors Somobrata Acharya and D.D. Sarma. She was a post-doctoral fellow in Prof. Yuval Golan's group at the Department of Materials Engineering, Ben Gurion University, Israel from March, 2013 to July, 2016. In 2017 she joined the Department of Physics, Mumbai University, India, as a DST Inspire Faculty Fellow before moving to her current position in late 2018. Her research interests include synthesis and characterization of advanced materials and heterojunctions for photovoltaic, thermoelectric and sensor applications. She is studying II–VI series semiconductors like PbS, CdS, CuS and SnS with narrow bandgaps for energy conversion research. Fabrication of heterojunctions with Si NWs leads to enhanced device efficiency by effective electron-hole separation leading to prospective applications as light-harvesting devices.

Introduction

In today's world energy scenario with the fossil fuels fast depleting, more focus is given on greener renewable energy resources like solar, hydropower, and wind to reduce the carbon footprint [1, 2]. Solar energy is by far the most convincing alternative due to abundant availability and environment friendly nature. Although, till date, the first-generation solar cells comprising of silicon-based materials are the most efficient ones, slowly and steadily the other alternatives like thin-film photovoltaics are also gaining importance mainly because of their ease

of fabrication and flexibility [3, 4]. The second-generation solar cells comprising of cadmium telluride (CdTe) and copper indium gallium di-selenide (CIGS) [5, 6] showed initial promise, but they are usually associated with low cost-effectiveness and toxicity issues [7]. The emerging third-generation photovoltaics include copper zinc tin sulfide/ selenide and their derivatives (CZTS), dye sensitized solar cells (DSSCs), organic solar cell, perovskite solar cell, and quantum dots [8, 9]. Among these perovskites have received tremendous attention as their research efficiency was reported to be above 20% [10, 11].

Traditional single junction II–VI solar cells have a maximum theoretical efficiency of 33.16% popularly known as Shockley–Queisser limit. The efficiency of such solar cells is found to increase significantly under heterojunction configuration. Two different semiconductor layers of different bandgap, popularly referred to as "absorber" and "collector" or "window" layer, combine to form the HJ layer and the photocurrent produced predominantly due to the electrons generated in the depletion region in the absorber. Depending on the sequence of the constituent layers, these devices are configured mainly in two ways either superstrate structure or substrate structure [12, 13]. Further improvement of the efficiency results from the fabrication of multijunctional solar cell (MJ). MJ devices consist of different photoactive semiconductor layers with material bandgap spanning across a wide range of wavelengths in the solar spectrum. A schematic diagram describing the constituent layers of a typical MJ device is given in Fig. 1(a). Since the constituent junctions can efficiently extract power from the different portions of the solar spectrum, their power conversion efficiency is much higher compared to single p–n junction solar cells, and the tunnel junction controls the back flow of the electrons. Each of the constituting layers is associated with unique chemical and physical properties which synergistically contribute toward photocurrent thereby enhancing the overall performance of the resultant device.

Thin-film production remains the basis of HJ/MJ device fabrication and different deposition techniques such as sputtering, thermal evaporation, molecular beam epitaxy (MBE), chemical vapor deposition (CVD), and metal–organic chemical vapor deposition (MOCVD) which are quite popular [14–16]. Chemical bath deposition (CBD) is gaining significance because of its low cost, simplicity, uniformity, and ease of substrate choices. Additionally, multiple samples can be deposited in a single run [17, 18]. Thin films produced using CBD techniques find applications in optical imaging, solar window coating, and photovoltaics [19–23]. CBD usually includes direct deposition of the material onto the substrate with the precursors generated in the same bath [17]. The advantages of the CBD involves relatively low temperature and absence of any stringent conditions requiring very basic equipment like a hot plates, magnetic stirrers, hot water bath, and water-soluble salts. A typical CBD experimental setup is described schematically in Fig. 1(b). Control over the thickness and other physical and chemical properties of the film can be easily achieved by altering the growth parameters.

One of the earliest uses of the CBD includes the growth of cadmium sulfide (CdS) films over CdTe to improve the photovoltaic efficiency of the latter. Indeed, it was shown that the CdS grown by CBD over a CdTe thin film reported a higher efficiency than the cases where the CdS layer is grown by any other techniques [23–25]. Though over the years, this technique is successfully used to grow the different constituent layers in a HJ/MJ solar cell; to the best of our knowledge, the number of review articles describing the usage of CBD during the fabrication and their effect on the efficiency of HJ/MJ solar cell is sparse. This review is intended for summarizing the development in fabrication of heterojunction solar cells by CBD. A short description of the mechanism of CBD including the factors affecting the growth, a detailed description about the literature report of the different possible combinations of metal chalcogenide/ chalcopyrite for MJ solar cells followed by a summary, and a conclusion about the present-day scenario have been included here.

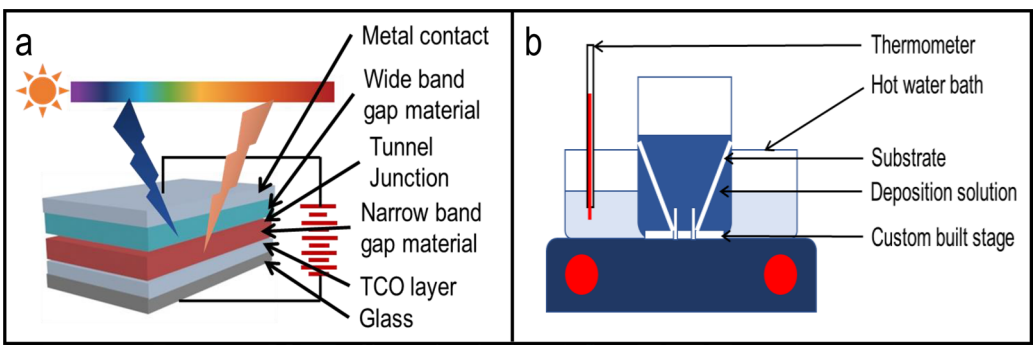

Figure 1: (a) Schematic diagram describing the constituent layers of a multijunctional (MJ) solar cell. (b) Schematic diagram of a typical chemical bath deposition (CBD) setup.

Mechanism of CBD and controlling factors

CBD became popular in the early 1940s for growing lead sulfide (PbS)-based infrared (IR) detectors [22]. In the following years, the number of materials deposited by CBD has increased significantly and now includes various metal chalcogenides, metal oxides, and chalcopyrite materials [17]. Typically, for growing a thin film of AB, the growth solution would usually consist of an aqueous solution of group II metal salts (A^{2+}), chalcogenide source from group VI (B^{2-}), hydroxide, and the complexing agents. The formation of the AB thin film involves the following three basic steps:

1. Dissociation and adsorption of metal complex on the substrates (A).
2. Hydrolysis of chalcogenides (B).
3. Evolution/growth of the solid thin films.

First step involves the dissociation of metal complex ions allowing control over the rate of the release of the metal ion. The pH and the temperature of the solution play an important role in controlling the rate of the subsequent steps, like hydrolysis of chalcogenides (B) and growth of the solid thin films.

There are basically two broad mechanisms which follow during the operation of CBD [17]:

1. Ion-by-Ion mechanism: Here, the growth occurs by decomposition of chemical precursors only at solid surface not in bulk solutions.
2. Cluster mechanism: The growth of the films occurs by migration and adsorption of colloidal particles.

The factors determining which mechanism will be operating include the temperature, pH, and the presence of complexing agents [26]. At lower temperature for a given deposition solution due to the presence of greater number of nucleation on the substrate surface, the resultant crystallite size is expected to be smaller. Contrarily, at higher temperature, faster diffusion usually results in large crystallite size. Additional complexing agents like small-chain organic acids and amines are added to the solutions, which effectively complexes the metal ions leading to its slow release and thereby influencing the resultant film quality [27]. The most used complexing agents include tri-sodium citrate, tri-ethyl ammonia (TEA), tartaric acid, and ethylenediaminetetraacetic acid (EDTA). The thin films grown by cluster mechanisms are associated with amorphous nature and smaller crystalline size compared to those grown by ion-by-ion reaction. An intricate balance between all the parameters is necessary to achieve a successful film growth.

A modified version of CBD is known as successive ion layer adsorption and reaction (SILAR) in which the substrate is alternatively dipped in two different precursor solutions with intermediate rinsing [28–30]. This ideally results in the formation of the single monolayer of the desired compound and subsequent film growth.

HJ/MJ solar cells deposited by CBD

MJ solar cells consist of multiple p-n junctions made of different semiconductor materials. The choice of materials for each subcell is determined by the lattice and electrical matching between the constituent layers. Though the commercially available tandem solar cells comprise of III-V semiconductors, their electrical properties are highly sensitive to dislocations and other structural defects associated with the lattice mismatching of the constituent layers. On the contrary, such structural defects have a minor effect on the electronic properties of the II–VI materials due to the more ionic nature of them though they are associated with stability issues and formation of contacts [31, 32]. Literature reports suggest that suitable combinations of metal chalcogenides and chalcopyrite materials deposited by CBD show encouraging results as plausible HJ/MJ solar cells [22]. The following sections are described in detail HJ/MJ photovoltaic cells with different combinations fabricated by CBD. For the sake of convenience, we have classified the discussion according to the main absorber layer and discussed the respective combinations of different buffer layers.

Cadmium telluride (CdTe)

CdTe is the most promising second-generation photovoltaic material with a direct bandgap of 1.5 eV. [33–35] Historically, CdTe was combined with CdS buffer layer for improved efficiency [36–42]. Chu et al. were first to report CdS/CdTe HJ thin-film solar cell by CBD with ~ 13.4% efficiency as early as 1991 [25]. p-CdTe of 3–5 μm thickness was deposited by closed-spaced sublimation (CSS) over 50–150 nm CdS buffer layer deposited from the bath consisting of an ammonia solution of a Cd-salt, an ammonium salt, and thiourea. The thickness and the properties of the constituting layers were optimized by controlling the temperature and the precursor concentrations. The resultant heterojunction solar cell of 1.2 cm^2 area under global 1.5 illumination was found to have an open-circuit voltage (V_{OC}), short-circuit current density (J_{SC}), and fill factor (FF), and their values are 0.84 V, 21.9 mA/cm^2, and 72.6%, respectively, corresponding to a conversion efficiency of 13.4%, much higher than the films deposited by other methods. The maximum efficiency achieved for such a structure was reported to be ~ 16.2% by Wu et al. [33, 43] The following development in CdS/CdTe HJ solar cell efficiency approaching the efficiency limit has been summarized by

Morales-Acevedo in his review article [44]. He discussed by improving the V_{OC} and FF, a maximum efficiency of ~ 17.5% can be achieved but such a structure has limitations related to contact resistivity, stability, and reliability of the ohmic contacts on CdTe. Lately, Yang et al. discussed in detail how the CdS/CdTe junction quality and the resultant efficiency critically depend on the annealing atmosphere of the CdS window layer [45]. Highly crystalline CdS films with only one monograined layer with a thickness of several tens of nanometers could be obtained and successfully employed as buffer layer to increase the efficiency. CdS precursor films were coated with a $CdCl_2$ layer followed by thermal treatment in the presence of $CdCl_2$ and air to avoid over-oxidation during the further deposition process [Fig. 2(a)]. Such thermal treatments results in significant increase in the J_{SC} due to reduced carrier scattering at grain boundaries and enhanced light transmission. The subsequent CdTe deposition resulted in almost in a perfect junction devoid of pin holes [Fig. 2(b)]. Upon heat treatment under a high $CdCl_2$ vapor pressure, over-oxidation at the grain surface is reduced which promotes in-plane grain coalescence along the CdS/FTO (F-doped SnO_2) interface ensuring homogeneous intermixing of CdS and CdTe at the junction interface. A reduced external quantum efficiency was observed when the cell was fabricated with a dip-coating CdS layer rather than coating vapor, since, in the case of dip-coating, inappropriate junction results in pinholes formation which affects the resultant electric field because of reduced junction area and enhanced recombination for carriers generated deep in CdTe layer [Fig. 2(c)]. The corresponding solar cell with monograined CdS layer had an efficiency of 14.6%.

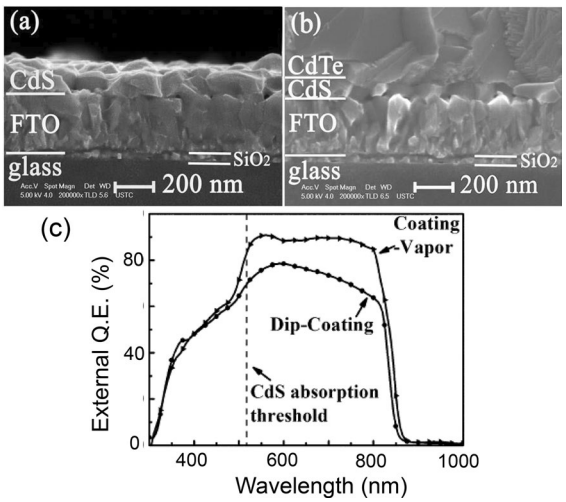

Figure 2: (a) Cross-sectional SEM morphology of CdS film fabricated by the coating-vapor method; (b) Cross-sectional SEM morphology of CdTe/CdS cell junction. (c) Comparison of the external quantum efficiencies for the two CdTe solar cells having 80 nm-thick CdS window layers prepared by the dip-coating and coating-vapor methods, respectively. (Reproduced from Ref. [45] with the permission from Royal Society of Chemistry).

To improve the efficiencies of the CdS/CdTe HJ solar cell, researchers tried to incorporate additional buffer layers for reducing leakage currents. Incorporation of TiO_2 buffer layer in-between thin semiconducting layer and the front contact improved the resultant efficiency. Mutalikdesai et al. fabricated semi-transparent TiO_2/CdS/CdTe HJ solar cells and initial cell exhibited a voltage of 100.53 mV and photocurrent of 14.7 mA/cm^2 illustrating the potential of the process [46]. Other transparent metal oxides such as zinc oxide (ZnO) and TiO_2 can also be explored [47].

In order to increase the efficiency of the CdTe solar cell, alternate buffer layers replacing conventional CdS layer are explored [48]. Cadmium selenide (CdSe) with a lower bandgap may not be suitable to substitute CdS; however, the solubility of the CdSe in CdTe is expected to be much higher than that of CdS leading to higher inert diffusion at the interface during CdTe deposition and post-deposition treatment. Additionally, $CdTe_{1-x}Se_x$ alloys are formed in the interface which has lower bandgap than that of CdTe which in turn leads to an increase in J_{SC}. There are interesting reports regarding the performance of CdTe solar cell with CdSe or a bilayer of CdS/CdSe as the n-type heterojunction partner [49–51]. Paudel et al. reported enhanced J_{SC} in both short- and long-wavelength regions by using CdSe as the window layer [52]. The presence of combined CdS/CdSe window layer leads to high V_{OC} and maintains the J_{SC} enhancements. However, these structures are fundamentally limited due to the diffusion of the Se into the CdS layer, leading to the potential formation of parasitic $CdS_{(1-x)}Se_x$ phases and hence a decrease in J_{SC}. Baines et al. optimized SnO_2/CdSe/CdTe HJ cell structure to an efficiency of 13.5%, the reduced efficiency resulting due to lower V_{OC}. Their investigations suggested replacing the SnO_2 layer with other alternative oxides like TiO_2, ZnO, and FTO is the key to overcome the V_{OC} deficit [50]. Recently, Morris et al. successfully controlled the particle size, surface coverage, and thickness of CBD-grown CdSe layer and were made into full devices with CdTe [49]. The resultant alloyed compound $CdTe_{1-x}Se_x$ at the interface shows both improved external quantum efficiency (EQE) and J_{SC} in the IR wavelengths. The resultant device is found to have a maximum efficiency of 12.3% with a film thickness of 280 nm and grain size of ~ 600 nm.

Lead sulfide (PbS)/lead selenide (PbSe)

PbS has emerged as the prospective candidate for photovoltaic application because of its absorption in the longer wavelength (near IR region) which can be further tuned owing to the quantum size effect [53, 54]. While PbS quantum dots have drawn significant attention, only a handful of reports are available for the fabrication of PbS-based solar cells [55–60]. CdS/PbS heterostructures were first reported in 1970s by spray pyrolysis

method with a V_{OC} of 400 mV and J_{SC} of 0.04 mA/cm^2 [61]. Hernandez-Borja et al. first reported glass/ITO/CdS/PbS/conductive graphite fabricated entirely by CBD process [62]. CdS window layers were deposited using CBD in the presence of different complexing agents. The as-fabricated solar cells are photosensitive in a large spectral range (all visible and near infrared regions) and had an efficiency of 1.63%. Their studies also revealed that altering the complexing agent during the deposition does not affect the efficiency of the overall structure. Later, Obaid et al. prepared n-CdS/p-PbS heterojunction solar cells via microwave-assisted CBD [63]. Different thicknesses of PbS absorber layer (985–1380 nm) were grown with different molar concentrations over pre-formed CdS window layer of ~ 340 nm. In the absence of any post-deposition treatment, the efficiencies of the resultant cells range from 0.35 to 1.68%, with changing molar concentrations resulted in improved photovoltaic performance. Yeon et al. fabricated PbS-thin-film-based depleted MJ solar cells wherein two band-aligned junctions are stacked by CBD [64]. The proposed device structure is illustrated in Fig. 3(a) wherein PbS layers of bandgaps of 1.61 eV and 0.92 eV are stacked. The large bandgap PbS layer absorbs mainly the short wavelength photons while the relatively longer wavelength photons are absorbed by the narrow bandgap PbS [Fig. 3(b)]. This widening of the absorption spectra results in an enhancement of power conversion efficiency (PCE) of the resultant device from 3.10 to 4.03% [Fig. 3(c)]. The resultant device was also found to have better stability. The HJ/ MJ solar cell efficiency can be further improved to ~ 5.59% by replacing the traditional CdS layer by a very thin CdS layer supported by vertically aligned ZnO nanorods [65].

Recently, Pérez Gracía et al. explored the properties of PbS thin films deposited by SILAR method and applied in PbS/CdS HJ solar cells [66]. PbS/CdS heterojunctions were fabricated, and J-V characteristics were studied. Though the maximum efficiency was obtained for 40 cycles of SILAR, there was no direct relation of the efficiency with thickness and number of cycles. Other than CdS, metal oxides like NiO and TiO_2 are also reported as the window layer for HJ solar cell with PbS absorber layer [67]. Sengupta et al. have explored the possibility of exploring zinc telluride (ZnTe) as the buffer layer paired with PbS as the absorber layer [68]. A detailed structural and chemical analysis reveals that the growth conditions like temperature and the reagent concentrations have strong effects on the morphologies and the properties of the resultant films specially the interface. Precaution is required for growing PbS thin films on ZnTe layer to take account for ZnTe solubility in the alkaline solution during CBD. At higher temperature, the orientation relationship is directly dependent on the substrate with the PbS growing epitaxially on the textured ZnTe layer. At lower temperature, however, due to slow growth rate of the PbS film, partial dissolution of the ZnTe layer takes place; as a result, the epitaxial relationship is not translated to the following layers. For the PbS films grown at 30 °C, the dark field transmission electron microscopy (DF TEM) image constructed from the selected area electron diffraction (SAED) pattern of the ZnTe|PbS interface clearly shows the orientation relationship between (111) $_{Film}$ II (111) $_{substrate}$ with PbS layer adopting the underlying ZnTe grain orientation [Fig. 4(a, b)]. On the contrary, for the films grown at 20 °C, the interface clearly shows the dissolution of the constituent layers. Scanning transmission electron microscopy (STEM) images combined with energy-dispersive

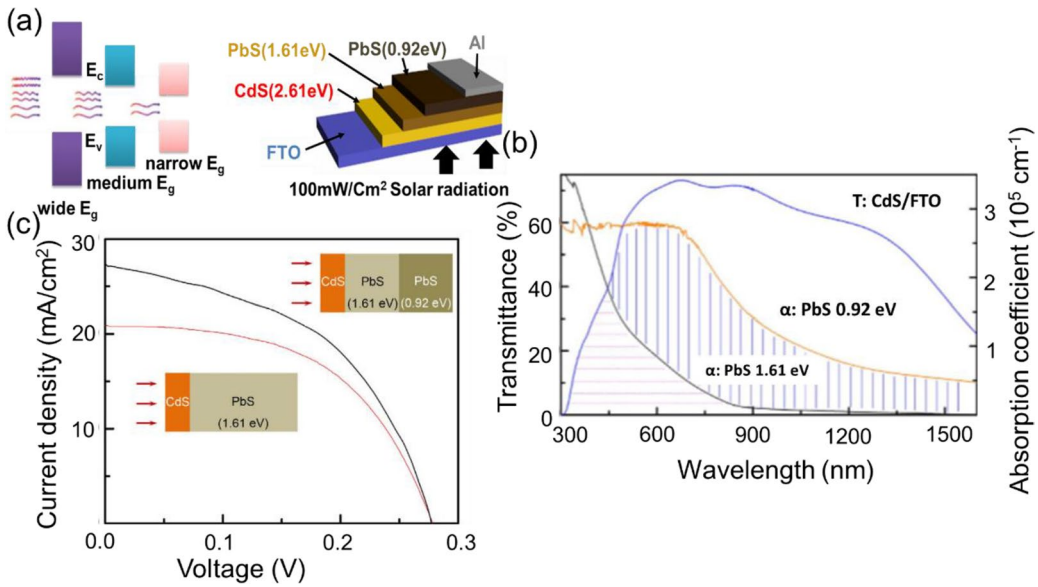

Figure 3: (a) Schematic diagram of the resultant device describing the constituent layers and their corresponding bandgap diagram. (b) Transmittance spectra of the CdS/FTO/Glass and absorption coefficient of PbS thin films with two different bandgaps of 0.92 and 1.61 eV. (c) Comparison of J–V plots of photovoltaic devices with a single PbS layer and with stacked layer. (Reproduced from Ref. [64] with the permission from Nature Research).

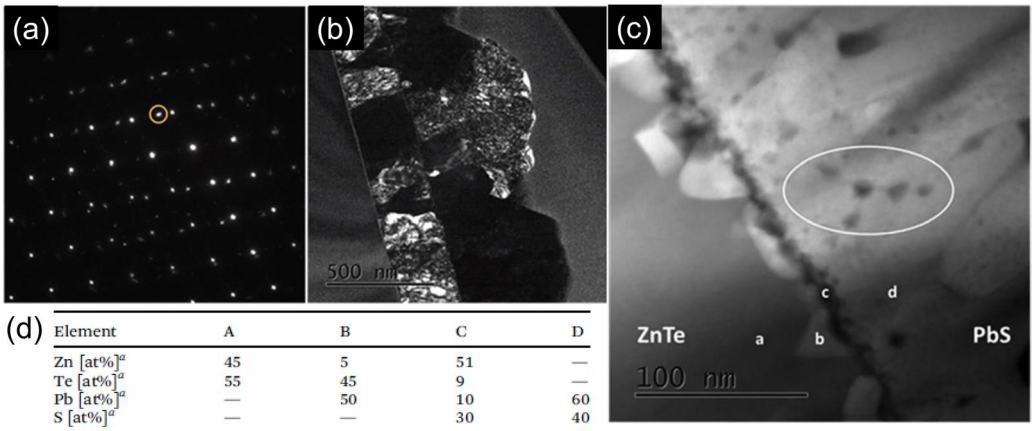

(d)

Element	A	B	C	D
Zn [at%][a]	45	5	51	—
Te [at%][a]	55	45	9	—
Pb [at%][a]	—	50	10	60
S [at%][a]	—	—	30	40

Figure 4: (a) SAED pattern of the ZnTe–PbS interface of the PbS/ZnTe/Si (100) structure, with the PbS film grown at 30 °C. in which the (11 $\bar{1}$) PbS reflection is encircled. (b) Corresponding DF -TEM micrograph. (c) HAADF STEM micrograph of the PbS–ZnTe interface with PbS film chemically deposited at 20 °C. and (d) Summary of STEM EDS analysis performed on the locations marked as a–d of the PbS–ZnTe films. (Reproduced from Ref. [68] with the permission from Royal Society of Chemistry).

X-ray spectroscopy (EDS) reveals the presence of PbTe nanocrystals along with a thin layer of nanocrystalline ZnS grains at the interface [Fig. 4(c, d)].

Similar to PbS, PbSe has also been not studied extensively as absorber layer in HJ/MJ solar cell deposited by CBD [69]. Nair et al. synthesized CdS/Sb_2S_3 heterojunction with or without PbSe absorber layer by using various source of selenium ions in bath such as sodium selenosulfate and N, N-dimethyl selenourea [70]. Without PbSe layer, it shows low current density, i.e.,0.03 mA/cm^2. PbSe thin film fabricated with N, N-dimethyl selenourea shows best value of 3.5 mA/cm^2 with FF of 0.28 and efficiency of 0.69. On the contrary, films developed by the pre-synthesized colloidal PbSe and CdS nanoparticles serve as a standard alternative synthetic route preferred over CBD [71–73]. CBD-deposited PbSe, however, finds a wide range of other applications, the most prevalent being mid-IR imaging sensors [74, 75].

Copper indium gallium sulfur/selenide (CIGS)

Copper indium selenide (CIS) and copper indium gallium selenide (CIGS)-based absorbers are potential candidates in photovoltaic technology due to their high energy conversion efficiency, low cost, and flexible module for thin-film solar cells [76–78]. The bandgap of pristine CIS layer is ~ 1 eV on upon incorporation of Ga, and the bandgap of CIGS varied from 1.04 to 1.7 eV [79, 80]. For fabrication of CIGS-based solar cell, buffer layer plays a vital role with absorber layer. An efficient pair of buffer layer would have similar electron affinities and compatible lattice structure with minimal lattice mismatch. In the section below, we intend to summarize a few of the most popular ones such as CdS, ZnS, and their effect on the resultant devices.

CdS buffer layers: So far, the most successful buffer layer in CIGS-based thin-film solar cell is with CBD-deposited CdS [81–84]. Pillai et al. fabricated HJ solar cell $CuInSe_2$/CdS by all CBD methods at room temperature [85]. From the result, they obtained best cell efficiency of 3.1%, and V_{OC} is 365 mV under illumination of 85mW/cm^2 on a cell of active area of 0.1 cm^2. The low efficiency of solar cell device was attributed due to high series resistance of the solution-grown CdS layer and low grain size of CIS layer. The interface between the CdS and CIGS layer is found to play a pivotal role in the resulting efficiency, and there are a few reports investigating the concerned interface. Schmid et al. proposed a model for the formation of an interfacial layer of defect chalcopyrite between p-type CIS and n-type CdS [86]. Thus intrinsically formed buried chalcopyrite/defect chalcopyrite is essential for the lattice matching of the heterojunctional partners. Kylner et al. demonstrated that apart from the interface, the bulk properties of the CdS layer above also plays an important role [87]. By increasing the impurity concentration or the thickness of the CBD-CdS layer, the V_{OC} was observed to substantially increase. When the CIGS devices were subjected to pre-deposition for an additional intermediate ultrathin layer, the resultant efficiencies were not much affected. Abou-Ras et al. compared the structural and chemical properties of the CdS buffer layer grown by two different methods viz. physical vapor deposition (PVD) and CBD [88]. PVD-CdS layers show much larger grain sizes, and the CIGS interface is abrupt with higher defect density owing to a higher lattice mismatch. On the other hand, CBD-CdS/CIGS interface is rather diffused and due to this interdiffusion of the Cd and In, an inversion of the near interface region from p-type to n-type CIGS occurs which is the reason for greater efficiencies compared to PVD-CdS. Simple spray

pyrolysis is successfully employed to deposit CIGS layer over CBD-grown CdS buffer layer to produce high-quality thin-film solar cells with 5.9% efficiency [89]. Similarly, CIGSSe layer can be deposited by spray pyrolysis over CBD-grown CdS layer resulting in solar cell efficiency of 10.5% under illumination [90].

ZnS buffer layer: Though the CdS buffer layers are quite efficient, however, they have serious toxicity issues associated with them. Zinc analogues are proposed as a suitable alternative to the CdS layer over the last few years [91–94]. The wider bandgap of ZnS (3.68 eV) makes it more transparent in the shorter wavelength region 350–550 nm which in turn improved the J_{SC} density of the device. Okamoto et al. studied the effect of zinc sulfide oxide Zn(O,S) buffer layer morphology and performance on CIGS solar cells varying the deposition time [95]. As the deposition time decreases, buffer layer thickness also decreases because of which surface roughness improves. They found improvement in conversion efficiency of CIGS photovoltaic cell from 6.75 to 13.67%. The cell efficiency of 15.50% obtained with V_{OC} of 0.65 V shows good cell performance of CIGS-based photovoltaics cell under optimized condition. Kobayashi et al. demonstrated the importance of the heat and light-soaking post-treatment for the ZnS(O, OH)/ CIGS solar cells which resulted in an efficiency of 18.8% [96]. Sun et al. deposited Zn(O,S) buffer layer by CBD over CIS absorber layer [97]. Reduction of the buffer layer thickness results in the increase in the PCE due to increase in the carrier lifetime. By optimizing the thickness and the quality of the buffer layer and the light-soaking post-treatment, an efficiency of 11.65% was obtained by Lin et al. without an anti-reflective coating layer [98]. The schematic structure of the fabricated CIGS is described in Fig. 5(a, b) and the corresponding cross-sectional SEM image in Fig. 5(c) which reveals uniform coverage of $Zn(S_{0.79}O_{0.21})$ on the rough CIGS surface. To investigate the effect of light soaking on the resultant efficiencies, experiments were done under AM1.5 light source at room temperature demonstrating highest efficiency of 11.65% [Fig. 5(d)]. Compared to that of the CIGS solar cell with CdS buffer layer, the value of J_{SC} was found to increase from 28.49 mA/cm^2 to 37.18 mA/cm^2 [Fig. 5(e)] due to increased optical absorption in the shorter wavelength region due to higher bandgap of Zn(S,O) than that of CdS [Fig. 5(f)]. They showed that the increase of the efficiency with the light-soaking time is mainly attributed to the increase in the FF. To clarify the mechanism, the carrier concentration (N_{CV}) is obtained from the C-V results along the depth direction from the Zn(S,O) buffer layer to CIGS absorber layer [Fig. 5(g)]. The tunneling-enhanced recombination in the space charge region and the interface recombination at the Zn (S, O)/CIGS interface are the dominant recombination mechanisms that affect the overall cell efficiency. The ratio of the oxygen to sulfur within the buffer layer is shown to be highly dependent on the zinc sulfide (ZnS) film deposition rate which in turn depends on the higher stability constant during decomplexation of the zinc ligands.

Hong et al. discussed the dependence of the different zinc precursor during the CBD deposition of the ZnS on the efficiency of the resultant CIGS solar cell, and zinc acetate was found to have the best cell efficiency of 9.4% [99]. Recently, Kim et al. demonstrated that the presence of additional complexing agent hydrazine hydrate also has immense effect on the physical characteristics of the ZnS buffer layer [100]. In the presence of

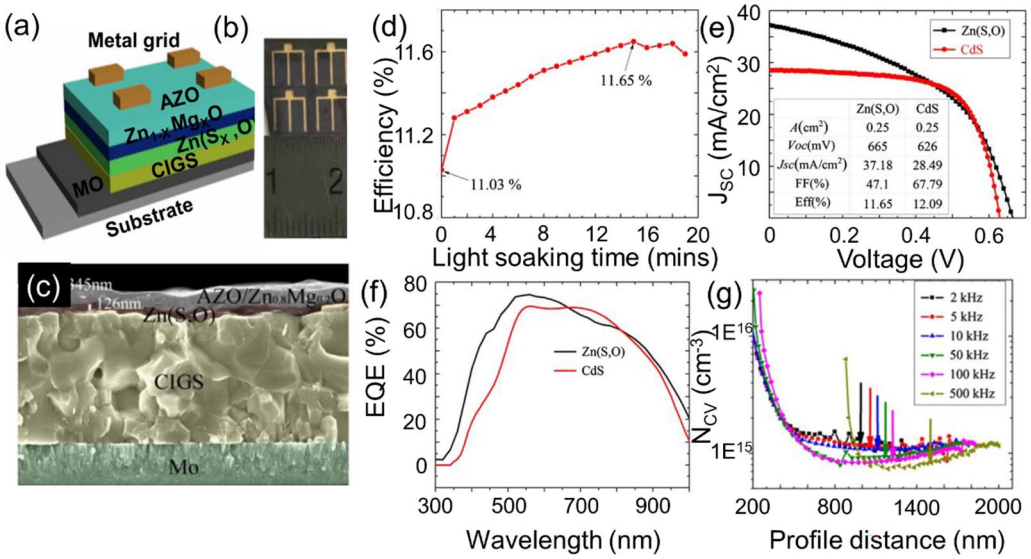

	Zn(S,O)	CdS
A(cm^2)	0.25	0.25
Voc(mV)	665	626
Jsc(mA/cm^2)	37.18	28.49
FF(%)	47.1	67.79
Eff(%)	11.65	12.09

Figure 5: (a) Schematic diagram of the structure of CIGS solar cell. (b) Real image of CIGS solar cells. (c) The cross-sectional SEM image of the resultant solar cell. (d) The efficiency of the resultant cell with variation in different light-soaking time. Comparison of J–V curves of optimal cell (e) and EQE (f) with Zn(S,O) buffer layer and reference cell with CdS buffer layer. (g) Space charge distribution at the p–n junction from the CBD-Zn(S,O) buffer to the CIGS absorber layer (Reproduced from Ref. [98] with the permission from Elsevier).

hydrazine, the ZnS buffer layer is found to have a composition of [S/(S + O)] ~ 0.32 and a direct energy bandgap of 3.54–3.75 eV. When paired with CIGS, the heterojunction device recorded the highest efficiency of 12.03% along with V_{OC} of 0.549 V and J_{SC} of 32.92 mA/cm^2.

Copper zinc tin sulfur/selenide (CZTS)

Copper zinc tin sulfur/selenide (CZTS) with a direct bandgap between 1.45 eV and 1.6 eV and large absorption coefficient is considered as a suitable candidate as the absorber layer for the next-generation thin-film solar cell mainly for the absence of toxic elements and cost reduction for mass production [101, 102]. During the early part of this decade, researchers reported the synthesis of the CZTS-based solar cell by CBD with CZTS as the absorber layer paired with CdS and ZnS as the buffer layer [103–106]. Gao et al. reported a low-cost method to fabricate CZTS-based solar cells by successively depositing the precursor layers (SnS, CuS, and ZnS) by CBD and subsequent annealing in a selenium atmosphere in the furnace [107]. By optimizing the growth conditions, one can achieve efficiencies of up to 4.5% on an area of 0.25 cm^2. While measuring the I-V characteristics of the CZTS solar cell with CdS as the buffer layer, they observed cross-over behavior which they believed to arise from an illumination-dependent electron barrier at the interface between the absorber and the buffer layer. Also, the interface recombination between the absorber and the buffer layer reduces the V_{OC} of the resultant device. Lin et al. also reported fabrication of CZTS- and CZTSe-based solar cells by similar method with an efficiency of 2.2% and 3%, respectively [103]. Recently, Sun et al. reported that the efficiency of the CZTS-based solar cell can be substantially improved by replacing the traditional CdS buffer layer with Zn-doped $Cd_{0.6}Zn_{0.4}S$ film [108]. The SEM images of the CdS thin films on CZTS show many pinholes and voids which are found to be improved after Zn-doping increasing the collection of the photogenerated carriers [Fig. 6(a, b)]. Compared to CdS/CZTS heterojunction, $Cd_{0.6}Zn_{0.4}S$/CZTS heterojunction has more appropriate band alignment with the conduction band offset reduced to 0.27 eV compared to 0.51 eV for CZTS/CdS [Fig. 6(c)] due to Zn-doping which is expected to be beneficial for carrier recombination and the photovoltaic performance. The better photovoltaic performance is achieved by the $Cd_{0.6}Zn_{0.4}S$/CZTS solar cells with the J_{SC} increased to 15.05 mA/cm^2 with a resulting efficiency of 4.88% [Fig. 6(d)].

Su et al. fabricated solar cell devices with the structure of Ag-glue/AZO/i-ZnO/CdS/CZCTS/Mo/glass and studied the effect of introduction of cadmium into the CZTS thin film

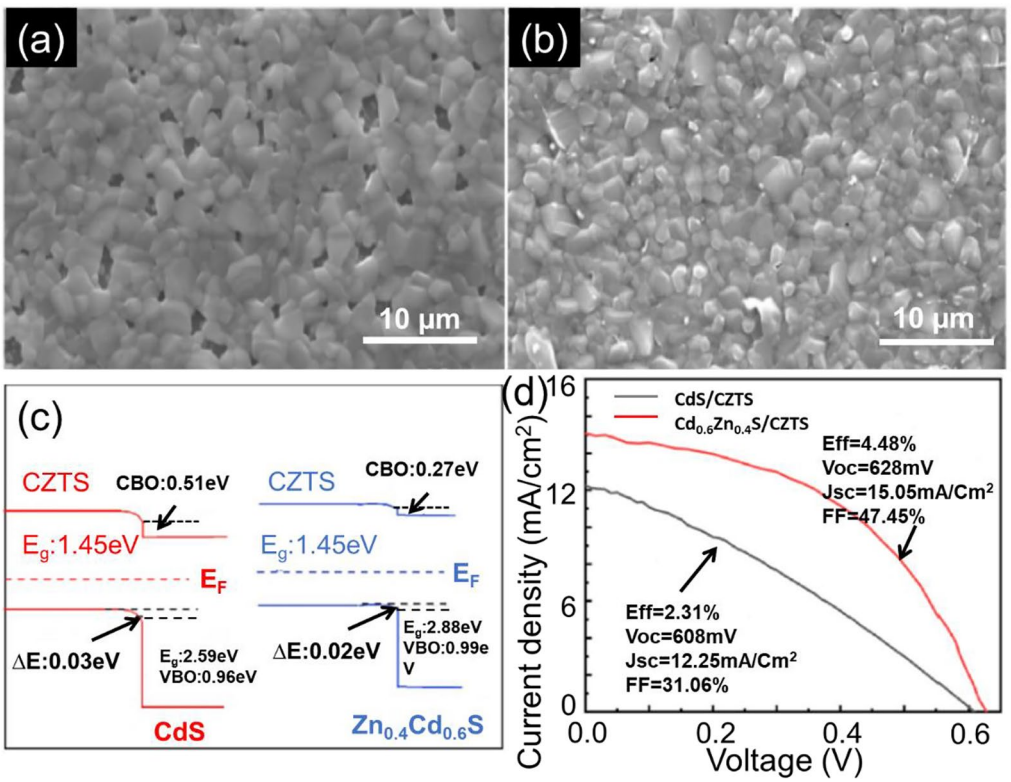

Figure 6: SEM images of the CdS (a) and $Cd_{0.6}Zn_{0.4}S$ (b) films. (c) Schematic diagram describing the band alignment of CZTS/CdS and CZTS/$Cd_{0.6}Zn_{0.4}S$ heterojunction with their corresponding bandgap values as calculated. (d) Comparison of J–V characteristics of the CZTS/CdS and CZTS/$Cd_{0.6}Zn_{0.4}S$ solar cells (Reproduced from Ref. [108] with the permission from Elsevier).

[109]. The bandgap and crystal structure of CZCTS thin film are affected by the change in the Zn/Cd ratio. With appropriate Zn/Cd ratio, the power efficiency of the resultant device increases to 9.24% due to the change in band alignment and subsequent charge separation at the CZCTS/buffer interface. Nguyen et al. demonstrated the successful use of a ZnS buffer layer for CZTSSe monograin solar cell [110]. Morphology, thickness, and the chemical composition of the ZnS buffer layer affect the resultant efficiency. Optimization study reveals a single layer of 10–25 nm ZnS to be most efficient with an efficiency of 4.5 (± 0.16) %.

In summary, the literature studies for different HJ/MJ solar cell along with their corresponding cell structure and the efficiencies are tabulated in the following Table 1. Analysis of the available literature references indicates variation in the buffer layer for CdTe and CIGS as the absorber layer in a HJ/MJ solar cell results in a maximum efficiency of ~ 19%.

Conclusion

In this review, we provided a comprehensive overview of the different II–VI semiconductor thin-film layers used as the absorber and the buffer layers in HJ/MJ solar cell structures by CBD. CBD especially SILAR method offers a simple and cost-effective method for fabrication of large-scale heterojunctional solar cell structure. Control over the growth parameters ensures better control over the film morphology specially at the interface. Special emphasis on the structural and elemental identification of interface is required to reduce the interfacial recombination to increase the J_{SC} and V_{OC} thus increasing the overall efficiency of the cell. The presence of impurity or introduction of the dopants in the buffer layer is found to reduce the lattice mismatch and the band offset between the heterojunction partners thereby resulting in an increased efficiency. The presence of interfacial defects at the heterojunctions is likely to produce defect states with forbidden bandgap increasing the band bending effects and

TABLE 1: Summary of the different MJ solar cells prepared by CBD and their corresponding efficiencies.

Sr No	Absorber layer	Buffer layer	Substrate	Efficiency %	References
1	CdTe	CdS	Glass/FTO/CdS/CdTe	13.4	[25]
			Glass/FTO/CdS/CdTe	15.8	[41]
			CTO/ZTO/CdS/CdTe	16.5	[43]
			Glass/FTO/CdS/CdTe	12.6	[36]
			Glass/TCO/CdS/CdTe	16.5	[44]
			Glass/FTO/CdS/CdTe	14.6	[45]
		CdSe	Glass/FTO/CdSe/CdTe	14.7	[52]
			FTO/SnO_2/CdSe/CdTe	13.5	[50]
			FTO/CdSe/CdTe	12.3	[49]
2	PbS	CdS	Glass/ITO/CdS/PbS	1.63	[62]
			Glass/ITO/CdS/PbS	1.68	[63]
			Glass/SnO_2/CdS/PbS	1.668	[59]
			Glass/FTO/CdS/PbS	3.10–4.03	[64]
			Glass/ITO/CdS/PbS	1.31	[57]
			Glass/ITO/CdS/PbS	0.127	[66]
3	PbSe	CdS	TCO/CdS/Sb_2S_3/PbSe	0.69	[70]
			Si/CaF_2/ PbSe/CdS	1.79	[75]
4	CIGS	CdS	SLG/MO/CIGS/CdS/ZnO/ITO/MgF_2	17	[81]
			SLG/FTO/CIS/CdS	3.1	[85]
			SLG/MO/CIGS/CdS/ZnO	19.2	[82]
			SLG/MO/CIGS/CdS/ZnO	14.6	[88]
			SLG/MO/CIGS/CdS/i-ZnO	17.22	[83]
			SLG/MO/CIGS/CdS/ZnO/ITO	18	[84]
		ZnS	SLG/MO/CIGS/ZnS/ZnO-Al/MgF_2	18	[94]
			SLG/CIGS/ZnS(O,OH)/ZnO	18.8	[96]
			SLG/MO/CIGS/Zn(O,S)	15.5	[95]
			SLG/MO/CIGS/ZnS	9.4	[99]
			Glass/MO/CIGS/Zn(S,O)/ZnMgO/AZO	11.65	[98]
			SLG/CIGS/ZnS	12.03	[100]
5	CZTS	CdS	SLG/MO/SnS/CuS/ZnS/CdS/ZnO	4.5	[107]
			Glass/ZnS/SnS_2/CuS	2.2–3.0	[103]
			SLG/MO/CZTS/CdZnS/i-ZnO/ITO	2.31–4.88	[108]

the recombination of excess minority carriers. Optimization of the interface between the heterojunction partners thus is crucial to improve the resultant cell parameters. SILAR method is favored over traditional CBD method since it offers a controlled exposure to the precursors resulting in a better control over the morphology. Another potential substitute can be the use of flow reactor for CBD where the fresh reactors are continuously fed into the reactor along with the simultaneous removal of the products. Although a limited number of papers indicate the initial optimization of this technique for pristine metal chalcogenide layers [110], they are yet to be exploited for the fabrication of HJ/MJ solar cells.

Acknowledgments

SS and RA acknowledge DST Inspire faculty award (DST INSPIRE 04/2016/000640) by the Ministry of Science& Technology, Government of India, for providing financial support.

Funding

Funding was provided by Department of Science and Technology, Ministry of Science and Technology (DST INSPIRE 04/2016/000640).

Data availability

Data sharing is not applicable to this article as no datasets were generated during the current study.

Declarations

Conflict of interest There is no conflict to declare.

Open Access

References

1. N. Asim, K. Sopian, S. Ahmadi, K. Saeedfar, M.A. Alghoul, O. Saadatian, S.H. Zaidi, Renew. Sustain. Energy Rev. **16**, 5834 (2012)
2. K.L. Chopra, P.D. Paulson, V. Dutta, Prog. Photovolt. **12**, 69–92 (2004)
3. R. Corkish, *Encyclopedia of Energy* (Elsevier, New York, 2004)
4. T. Soga, *Nanostructured Materials for Solar Energy Conversion* (Elsevier, New York, 2006)
5. M.A. Contreras, B. Egaas, K. Ramanathan, J. Hiltner, A. Swartzlander, F. Hasoon, R. Noufi, Prog. Photovolt. Res. Appl. **7**, 311 (1999)
6. M. Kemell, M. Ritala, M. Leskelä, Crit. Rev. Solid State Mater. Sci. **30**, 1 (2005)
7. A. Goetzberger, V. Hoffmann, *Photovoltaic Solar Energy Generation* (Springer, Berlin, 2005)
8. O.K. Simya, P. Radhakrishnan, A. Ashok, K. Kavitha, R. Althaf, *Handbook of Nanomaterials for Industrial Applications* (Elsevier, New York, 2018)
9. M.A. Green, Physics E **14**, 65 (2002)
10. E.H. Anaraki et al., Energy Environ. Sci. **350**, 2761 (2013)
11. G. Yang, H. Tao, P. Qin, W. Ke, G. Fang, J. Mater. Chem. A **4**, 3970 (2016)
12. F. Gaspari, S. Quaranta, *Comprehensive Energy Systems* (Elsevier, New York, 2018)
13. T. Kirchartz, D. Abou-Ras, U. Rau, *Advanced Characterizarion Techniques for Thin Film Solar Cells* (Wiley, Hoboken, 2016)
14. J. George, *Preparation of Thin Films* (CRC Press, Boca Raton, 1992)
15. K. Seshan, D. Schepis, *Handbook of Thin Film Deposition*, 4th edn. (Elsevier, New York, 2018)
16. L. Eckertova, *Physics of Thin Films* (Springer, Berlin, 1977)
17. G. Hodes, *Chemical Solution Deposition Of Semiconductor Films* (CRC Press, Boca Raton, 2002)
18. R.S. Mane, C.D. Lokhande, Mater. Chem. Phys. **65**, 1 (2000)
19. P.K. Nair, M. Ocampo, A. Fernandez, M.T.S. Nair, Sol. Energy Mater. **20**, 235 (1990)
20. P.K. Nair, V.M. Garcia, A.M. Fernandez, H.S. Ruiz, M.T.S. Nair, J. Phys. D **24**, 441 (1991)
21. P.J. Sebastiant, M. Pattabi, J. Phys. D **25**, 981 (1992)
22. P.K. Nair, M.T.S. Nair, V.M. García, O.L. Arenas, Y. Peña, A. Castillo, I.T. Ayala, O. Gomezdaza, A. Sánchez, J. Campos, H. Hu, R. Suárez, M.E. Rincón, Sol. Energy Mater. Sol. Cells **52**, 313 (1998)
23. T.L. Chu, S.S. Chu, Prog. Photovolt. Res. Appl. **1**, 31 (1993)
24. T.L. Chu, S.S. Chu, N. Schultz, C. Wang, C.Q. Wu, J. Electrochem. Soc. **139**, 2443 (1992)
25. T.L. Chu, S.S. Chu, C. Ferekides, C.Q. Wu, J. Britt, C. Wang, J. Appl. Phys. **70**, 7608 (1991)
26. F.G. Hone, T. Abza, Int. J. Thin Film Sci. Technol. **8**, 43 (2019)
27. S. Sengupta, R. Aggarwal, Y. Golan, Mater. Chem. Front. **5**, 2035 (2021)
28. H.M. Pathan, C.D. Lokhande, Bull. Mater. Sci. **27**, 85 (2004)
29. H. Unuma, T. Kanehama, K. Yamamoto, K. Watanabe, T. Ogata, M. Sugawara, J. Mater. Sci. **38**, 255 (2003)

30. M. Ristov, G. Sinadinovski, I. Grozdanov, M. Mitreski, Thin Solid Films **173**, 53 (1998)
31. J.W. Garland, T. Biegala, M. Carmody, C. Gilmore, S. Sivanan-than, J. Appl. Phys. **109**, 102423 (2011)
32. T.D. Lee, A.U. Ebong, Renew. Sustain. Energy Rev. **70**, 1286 (2017)
33. X. Wu, Sol. Energy **77**, 803 (2004)
34. A. Romeo, E. Artegiani, D. Menossi, Sol. Energy **175**, 9 (2018)
35. B.M. Basol, B. McCandless, J. Photonics Energy **4**, 040996 (2014)
36. R. Mendoza-Pérez, J. Aguilar-Hernández, J. Sastre-Hernán-dez, N. Ximello-Quiebras, G. Contreras-Puente, G. Santana-Rodríguez, O. Vigil-Galán, E. Moreno-García, A. Morales-Acevedo, Sol. Energy **80**, 682 (2006)
37. T. Sinha, L. Verma, A. Khare, Appl. Phys. A **126**, 867 (2020)
38. T. Sinha, D. Lilhare, A. Khare, J. Mater. Sci. **54**, 12189 (2019)
39. C. Ferekides, J. Britt, Sol. Energy Mater. Sol. Cells **35**, 255 (1994)
40. A. Ashok, G. Regmi, A. Romero-Núñez, M. Solis-López, S. Velumani, H. Castaneda, J. Mater. Sci. Mater. Electron. **31**, 7499 (2020)
41. J. Britt, C. Ferekides, Appl. Phys. Lett. **62**, 2851 (1993)
42. O. Vigil-GaÍn, A. Arias-Carbajal, R. Mendoza-Pérez, G. San-tana-Rodríguez, J. Sastre-Herńndez, J.C. Alonso, E. Moreno-García, G. Contreras-Puente, A. Morales-Acevedo, Semicond. Sci. Technol. **20**, 819 (2005)
43. X. Wu, J. C. Keane, R. G. Dhere, C. DeHart, D. S. Albin, A. Duda, T. A. Gessert, S. Asher, D. H. Levi and P. Sheldon, in *Proceedings of the 17th European PVSEC*, 995 (2001).
44. A. Morales-Acevedo, Sol. Energy **80**, 675 (2006)
45. R. Yang, L. Wan, D. Wang, D. Wang, RSC Adv. **4**, 22162 (2014)
46. A. Mutalikdesai, S.K. Ramasesha, Thin Solid Films **632**, 73 (2017)
47. R.W. Crisp, G.F. Pach, J.M. Kurley, R.M. France, M.O. Reese, S.U. Nanayakkara, B.A. Macleod, D.V. Talapin, M.C. Beard, J.M. Luther, Nano Lett. **17**, 1020 (2017)
48. X. Fang, S. Ren, C. Li, C. Li, G. Chen, H. Lai, J. Zhang, L. Wu, Sol. Energy Mater. Sol. Cells **188**, 93 (2018)
49. K. M. Morris, C. Potamialis, F. Bittau, J. W. Bowers and J. M. Walls, *Conf. Rec. IEEE Photovolt. Spec. Conf.*, 1857 (2019).
50. T. Baines, G. Zoppi, L. Bowen, T.P. Shalvey, S. Mariotti, K. Durose, J.D. Major, Sol. Energy Mater. Sol. Cells **180**, 196 (2018)
51. M.G. Reyes-Banda, E. Regalado-Perez, M.I. Pintor-Monroy, C.A. Hernández-Gutiérrez, M.A. Quevedo-López, X. Mathew, Superlattices Microstruct. **133**, 106219 (2019)
52. N.R. Paudel, Y. Yan, Appl. Phys. Lett. **105**, 183510 (2014)
53. P.K. Nair, M.T.S. Nair, A. Fernandez, M. Ocampo, J. Phys. D **22**, 829 (1989)
54. P.K. Nair, M.T.S. Nair, J. Phys. D **23**, 150 (1990)
55. H.M. Garcia, O. Gómez-Daza, J. Campos, M.T.S. Nair, P.K. Nair, Mater. Res. Soc. Symp. Proc. **1012**, 451 (2007)
56. N. Kavitha, R. Chandramohan, S. Valanarasu, T.A. Vijayan, S.R. Rosario, A. Kathalingam, J. Mater. Sci. Mater. Electron. **27**, 2574 (2016)
57. H. Sattarian, T. Tohidi, S. Rahmatallahpur, Mater. Sci. Pol. **34**, 540 (2016)
58. H.A. Mohamed, Sol. Energy **108**, 360 (2014)
59. D. Saikia, P. Phukan, Thin Solid Films **562**, 239 (2014)
60. R.A. Orozco-Terán, M. Sotelo-Lerma, R. Ramirez-Bon, M.A. Quevedo-López, O. Mendoza-González, O. Zelava-Angel, Thin Solid Films **343–344**, 587 (1999)
61. O.P. Agnihotri, B.K. Gupta, R. Thangaraj, Solid State Electron. **22**, 218 (1979)
62. J. Hernández-Borja, Y.V. Vorobiev, R. Ramírez-Bon, Sol. Energy Mater. Sol. Cells **95**, 1882 (2011)
63. A.S. Obaid, Z. Hassan, M.A. Mahdi, M. Bououdina, Sol. Energy **89**, 143 (2013)
64. D.H. Yeon, B.C. Mohanty, S.M. Lee, Y.S. Cho, Sci. Rep. **5**, 14353 (2015)
65. D.H. Yeon, B.C. Mohanty, C.Y. Lee, S.M. Lee, Y.S. Cho, ACS Omega **2**, 4894 (2017)
66. C.E. Pérez-García, S. Meraz-Dávila, G. Arreola-Jardón, F. De Moure-Flores, R. Ramírez-Bon, Y.V. Vorobiev, Mater. Res. Express **7**, 015530 (2020)
67. C. Augustine, M.N. Nnabuchi, R.A. Chikwenze, F.N.C. Any-aegbunam, C. Nwosu, C.O. Dike, C.V. Ezeh, B.J. Robert, E.M. Yohanna, E.N. Taddy, Chalcogenide Lett. **15**, 591 (2018)
68. S. Sengupta, T. Templeman, C. Chen, E. Moon, M. Shandalov, V. Ezersky, J. Phillips, Y. Golan, J. Mater. Chem. C **4**, 1996 (2016)
69. E. Barrios-Salgado, M.T.S. Nair, P.K. Nair, R.A. Zingaro, Thin Solid Films **519**, 7432 (2011)
70. P.K. Nair, E. Barrios-Salgado, J. Capistrán, M.L. Ramón, M.T.S. Nair, R.A. Zingaro, J. Electrochem. Soc. **157**, D528 (2010)
71. J. Zhang, J. Gao, C.P. Church, E.M. Miller, J.M. Luther, V.I. Klimov, M.C. Beard, Nano Lett. **14**, 6010 (2014)
72. L. Hu, X. Geng, S. Singh, J. Shi, Y. Hu, S. Li, X. Guan, T. He, X. Li, Z. Cheng, R. Patterson, S. Huang, T. Wu, Nano Energy **64**, 1 (2019)
73. W. Ahmad, J. He, Z. Liu, K. Xu, Z. Chen, X. Yang, D. Li, Y. Xia, J. Zhang, C. Chen, Adv. Mater. **31**, 1900593 (2019)
74. M.H. Jang, S.S. Yoo, M.T. Kramer, N.K. Dhar, M.C. Gupta, Semicond. Sci. Technol. **34**, 065009 (2019)
75. B. Weng, J. Qiu, L. Zhao, C. Chang, Z. Shi, Appl. Phys. Lett. **104**, 121111 (2014)
76. P. Jackson, R. Wuerz, D. Hariskos, E. Lotter, W. Witte, M. Pow-alla, Phys. Status Solidi. **10**, 583 (2016)
77. H.R. Moutinho, S. Johnston, B. To, C.S. Jiang, C. Xiao, P. Hacke, J. Moseley, J. Tynan, N.G. Dhere, M.M. Al-Jassim, Sol. Energy **161**, 235 (2018)
78. N. Naghavi, D. Abou-Ras, N. Allsop, N. Barreau, S. Bücheler, A. Ennaoui, C.H. Fischer, C. Guillen, D. Hariskos, J. Herrero,

R. Klenk, K. Kushiya, D. Lincot, R. Menner, T. Nakada, C. Platzer-Björkman, S. Spiering, A.N. Tiwari, T. Törndahl, Prog. Photovolt. Res. Appl. **18**, 411 (2010)
79. M. Gloeckler, J.R. Sites, J. Phys. Chem. Solids **66**, 1891 (2005)
80. M. Asaduzzaman, M. Hasan, A.N. Bahar, Springerplus **578**, 2256 (2016)
81. Y. Hashimoto, N. Kohara, T. Negami, N. Nishitani, T. Wada, Sol. Energy Mater. Sol. Cells **50**, 71 (1998)
82. K. Ramanathan, M.A. Contreras, C.L. Perkins, S. Asher, F.S. Hasoon, J. Keane, D. Young, M. Romero, W. Metzger, R. Noufi, J. Ward, A. Duda, Prog. Photovolt. Res. Appl. **11**, 225 (2003)
83. H. Komaki, A. Yamada, K. Sakurai, S. Ishizuka, Y. Kamikawa-Shimizu, K. Matsubara, H. Shibata, S. Niki, Phys. Status Solidi Appl. Mater. Sci. **206**, 1072 (2009)
84. T. Negami, Y. Hashimoto, S. Nishiwaki, Sol. Energy Mater. Sol. Cells **67**, 331 (2001)
85. P.K.V. Pillai, K.P. Vijayakumar, Sol. Energy Mater. Sol. Cells **51**, 47 (1998)
86. D. Schmid, M. Ruckh, F. Grunwald, H.W. Schock, J. Appl. Phys. **73**, 2902 (1993)
87. A. Kylner, J. Appl. Phys. **85**, 6858 (1999)
88. D. Abou-Ras, G. Kostorz, A. Romeo, D. Rudmann, A.N. Tiwari, Thin Solid Films **480–481**, 118 (2005)
89. J.C.W. Ho, T. Zhang, K.K. Lee, S.K. Batabyal, A.I.Y. Tok, L.H. Wong, A.C.S. Appl, Mater. Interfaces **6**, 6638 (2014)
90. M.A. Hossain, T. Zhang, L.K. Keat, X. Li, R.R. Prabhakar, S.K. Batabyal, S.G. Mhaisalkar, L.H. Wong, J. Mater. Chem. A **3**, 4147 (2015)
91. T. Ashrafee, K. Aryal, G. Rajan, S. Karki, V. Ranjan, A. Rockett, R. W. Collins and S. Marsillac, *Conf. Rec. IEEE Photovolt. Spec. Conf.* 1418 (2016).
92. T.M. Hsieh, S.J. Lue, J. Ao, Y. Sun, W.S. Feng, L.B. Chang, J. Power Sources **246**, 443 (2014)
93. W.J. Lee, H.J. Yu, J.H. Wi, D.H. Cho, W.S. Han, J. Yoo, Y. Yi, J.H. Song, Y.D. Chung, A.C.S. Appl, Mater. Interfaces **8**, 22151 (2016)
94. T. Nakada, M. Mizutani, Jpn. J. Appl. Physics **41**, L165 (2002)
95. T. Okamoto, H. Komaki, J. Sasano, S. Niki, M. Izaki, Energy Procedia **60**, 43 (2014)
96. T. Kobayashi, Z.J.L. Kao, T. Nakada, Sol. Energy Mater. Sol. Cells **143**, 159 (2015)
97. J. Sun, V. Nalla, M. Nguyen, Y. Ren, S.Y. Chiam, Y. Wang, K.F. Tai, H. Sun, N. Zheludev, S.K. Batabyal, L.H. Wong, Sol. Energy **115**, 396 (2015)
98. X. Lin, H. Li, F. Qu, H. Gu, W. Wang, Sol. Energy **171**, 130 (2018)
99. J. Hong, D. Lim, Y.J. Eo, C. Choi, Appl. Surf. Sci. **432**, 250 (2018)
100. J. Kim, C.R. Lee, V.K. Arepalli, S.J. Kim, W.J. Lee, Y.D. Chung, Mater. Sci. Semicond. Process. **105**, 104729 (2020)
101. H. Katagiri, N. Sasaguchi, S. Hando, S. Hoshino, J. Ohashi, T. Yokota, Sol. Energy Mater. Sol. Cells **49**, 407 (1997)
102. F. Zhou, F. Zeng, X. Liu, F. Liu, N. Song, C. Yan, A. Pu, J. Park, K. Sun, X. Hao, A.C.S. Appl, Mater. Interfaces **7**, 22868 (2015)
103. J. Li, G. Chen, C. Xue, X. Jin, W. Liu, C. Zhu, Sol. Energy Mater. Sol. Cells **137**, 131 (2015)
104. M. Cao, L. Li, B.L. Zhang, J. Huang, L.J. Wang, Y. Shen, Y. Sun, J.C. Jiang, G.J. Hu, Sol. Energy Mater. Sol. Cells **117**, 81 (2013)
105. S.S. Fouad, I.M. El Radaf, P. Sharma, M.S. El-Bana, J. Alloys Compd. **757**, 124 (2018)
106. A. Wangperawong, J.S. King, S.M. Herron, B.P. Tran, K. Pangan-Okimoto, S.F. Bent, Thin Solid Films **519**, 2488 (2011)
107. C. Gao, T. Schnabel, T. Abzieher, C. Krämmer, M. Powalla, H. Kalt, M. Hetterich, Thin Solid Films **562**, 621 (2014)
108. S. Sun, J. Guo, R. Hao, A. Aierken, B. Liu, K. Gu, L. Wang, X. Ma, G. Wei, J. Cai, H. Liu, X. Li, Y. Wang, Opt. Mater. (Amst) **112**, 110666 (2021)
109. Z. Su, J.M.R. Tan, X. Li, X. Zeng, S.K. Batabyal, L.H. Wong, Adv. Energy Mater. **5**, 1500682 (2015)
110. M. Nguyen, K. Ernits, K.F. Tai, C.F. Ng, S.S. Pramana, W.A. Sasangka, S.K. Batabyal, T. Holopainen, D. Meissner, A. Neisser, L.H. Wong, Sol. Energy **111**, 344 (2015)